Earth and Planetary Science Letters 554 (2021) 116667

Contents lists available at ScienceDirect

Earth and Planetary Science Letters

www.elsevier.com/locate/epsl

Billion-year exposure ages in Gale crater (Mars) indicate Mount Sharp formed before the Amazonian period

Peter E. Martin [a,*,1], Kenneth A. Farley [a], Charles A. Malespin [b], Paul R. Mahaffy [b], Kenneth S. Edgett [c], Sanjeev Gupta [d], William E. Dietrich [e], Michael C. Malin [c], Kathryn M. Stack [f], Paulo M. Vasconcelos [g]

[a] California Institute of Technology, Pasadena, CA, United States of America
[b] Goddard Space Flight Center, Greenbelt, MD, United States of America
[c] Malin Space Science Systems, San Diego, CA, United States of America
[d] Imperial College London, London, UK
[e] University of California Berkeley, Berkeley, CA, United States of America
[f] Jet Propulsion Laboratory, Pasadena, CA, United States of America
[g] University of Queensland, Brisbane, QD, Australia

ARTICLE INFO

Article history:
Received 17 July 2020
Received in revised form 13 October 2020
Accepted 4 November 2020
Available online 16 November 2020
Editor: W.B. McKinnon

Keywords:
Mars
Curiosity
geochronology
exposure dating
geomorphology

ABSTRACT

The erosion rates and mechanisms operating on Mount Sharp in Gale crater, Mars were assessed via experiments performed by the SAM instrument to determine the cosmogenic noble gas contents of Murray mudstone formation samples Mojave 2 and Quela. Previous measurements of samples from the Aeolis Palus depression between Mount Sharp and the north rim of Gale crater indicate that scarp retreat-generated surfaces formed within the last 100 Ma. In contrast, Mojave 2 yielded exposure ages of 1,320±240 (^{3}He), 910±420 (^{21}Ne), and 310±60 Ma (^{36}Ar). Quela gave a ^{3}He age of 1,460±200 Ma; ^{21}Ne and ^{36}Ar from this sample could not be quantified due to isobaric interferences. The discordant and young ^{36}Ar exposure age in Mojave 2 is likely the result of interaction with water which dissolved the chlorine-bearing host phases of this nuclide. The most probable exposure scenario is that both Mojave 2 and Quela have been at the surface for the most recent ~1 Ga after the overlying few meters of rock were removed in a geologically rapid exhumation episode. Based on local geomorphology, scarp retreat is the most likely mechanism for the exposure at these two sites. The exposure ages measured throughout Curiosity's traverse indicate that the net removal of rock has proceeded more recently on Aeolis Palus than on the lower slopes of Mount Sharp. The implied differential erosion rate is insufficient to explain how Mount Sharp formed, even over billions of years. Instead, given that the surfaces on Mount Sharp have existed for >1 Ga, the mountain must have formed early, likely during the Hesperian. This study provides direct quantitative support for inferences based on crater counts that Mount Sharp had eroded to close to its current form before onset of the Amazonian.

1. Introduction

The rates and dominant mechanisms of erosion on Mars are of interest to applications in crater dating (e.g., Malin et al., 2006), constraining the timing and rates of climate change (Golombek and Bridges, 2000), the geomorphic evolution of Martian surface features (Arvidson et al., 1979), and the search for pristine organic biosignatures (Pavlov et al., 2012). Modern-day erosion is thought to proceed on a long timescale, leaving some landforms largely unchanged for billions of years (Arvidson et al., 1979; Golombek and Bridges, 2000), although rapid erosion may occur locally on Mars (Grindrod and Warner, 2014).

Two previous noble gas cosmic ray exposure ages derived from data collected by the Sample Analysis at Mars (SAM; Mahaffy et al., 2012) and Alpha Particle X-ray Spectrometer (APXS; Gellert et al., 2015) instruments on the Mars Science Laboratory Curiosity rover confirmed the existence of young surfaces in Gale crater, where exposure ages of <100 Ma were detected (Farley et al., 2014; Vasconcelos et al., 2016). Both studies were performed early during the Curiosity rover mission at low elevations in Gale crater, before Curiosity reached Mount Sharp (formally, Aeolis Mons). Here we

* Corresponding author.
E-mail address: peter.martin-2@colorado.edu (P.E. Martin).
[1] Present address: University of Colorado Boulder, Boulder, CO.

https://doi.org/10.1016/j.epsl.2020.116667
0012-821X/

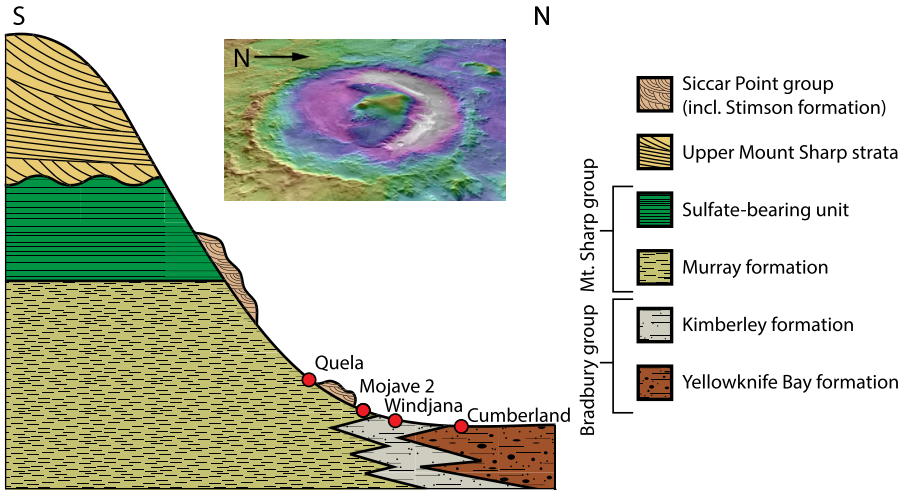

Fig. 1. Conceptual cross-sectional view of the Gale sedimentary sequence with sample locations noted. Inset shows topography of Gale Crater (credit: NASA/JPL/ASU/MSSS/GSFC); crater diameter is 154 km. The diagram is meant only to illustrate the relative stratigraphic position of each unit and is not to scale. See Grotzinger et al. (2015) for a description and to-scale diagram of all Gale crater units.

analyze the cosmogenic noble gases in two Mount Sharp samples, Mojave 2 and Quela, to assess the erosion rates operating on the lower slopes of Mount Sharp, and to evaluate when Mount Sharp formed.

1.1. Geologic setting

Gale crater is a 154 km-diameter impact crater formed no later than 3.6 Ga (Le Deit et al., 2013; Thomson et al., 2011). Gale contains sedimentary rock strata exposed in a 5.2 km-high mound, Mount Sharp, and in a depression north of the mound that separates it from the crater walls. The layered sediment which comprises Mount Sharp is not a central peak produced during impact (Bennett and Bell, 2016); it is similar to likely sedimentary mounds observed in craters across Mars (Bennett and Bell, 2016; Malin and Edgett, 2000). Fig. 1 is a conceptual cross-section of the major stratigraphic units exposed in northern Gale crater. The sedimentary sequence consists of rocks exposed on a relatively flat region termed Aeolis Palus, which includes the lowest-elevation rocks explored by Curiosity, referred to as the Bradbury group (Grotzinger et al., 2015). The Bradbury group contains the Yellowknife Bay and Kimberley formations, which are the source of the previously dated Cumberland and Windjana samples (Farley et al., 2014; Vasconcelos et al., 2016), respectively. The Bradbury group consists mostly of fluvial conglomerates and sandstones, interpreted as alluvial, fluvial, and deltaic sediments (Grotzinger et al., 2015). Grotzinger et al. (2015) interpreted Bradbury group rocks as older than the rocks of the Mount Sharp group exposed on lower Mount Sharp. Lower Mount Sharp is composed of the Murray formation, interpreted to largely be the lacustrine counterpart to the primarily fluviodeltaic sediments of the Bradbury group (Grotzinger et al., 2015). Above the Murray formation, a stratified sulfate-bearing interval forms the upper portion of the Mount Sharp group (Fraeman et al., 2016; Milliken et al., 2010). Above the Mount Sharp group lies ∼4.2 kilometers of unnamed strata thought to be of mostly eolian origin, forming the upper portion of the mound (Anderson et al., 2018; Milliken et al., 2010). The Siccar Point group is an additional sedimentary unit that unconformably overlies the Mount Sharp group at an interface called the Siccar Point unconformity and includes the eolian Stimson formation (Banham et al., 2018; Fraeman et al., 2016; Kronyak et al., 2019; Watkins et al., 2016). The time interval between the formation of Mount Sharp and the deposition of the Stimson formation is poorly constrained (Banham et al., 2018).

The rocks that compose Mount Sharp may have formed via sedimentary infilling of Gale crater followed by lithification (Day et al., 2016; Malin and Edgett, 2000). At some later point, an erosive regime began and the sedimentary rock that had filled Gale crater was broken down and removed from the basin. Impact craters, canyons, and yardangs on the slopes of Mount Sharp, and a large landslide deposit on the northeast side of the mountain, indicate that fragmentation by impact events plus fluvial, mass movement, and wind erosion all contributed to the shaping of Mount Sharp (Anderson and Bell, 2010; Day and Kocurek, 2016; Malin and Edgett, 2000). Wind was the likely agent responsible for removal of debris from Gale crater as the lithified fill material was disaggregated (Day et al., 2016). After Mount Sharp eroded to nearly its current shape, the Siccar Point group was deposited unconformably on the rocks of Mount Sharp (Fraeman et al., 2016). Small gullies, fans, and delta deposits distributed both on lower Mt. Sharp and on the crater rim might post-date Siccar point group deposition and could thus indicate periods of renewed water erosion and late episodic lake formation in Gale crater (Anderson and Bell, 2010; Grant and Wilson, 2019; Palucis et al., 2016, 2014; Wiens et al., 2020).

1.2. Cosmic ray exposure dating

Cosmogenic nuclides are produced in the upper 2-3 m of the Martian surface by nuclear interactions of galactic cosmic rays (GCRs) with the atoms in rocks (Fig. 2). We measured nuclides generated by two mechanisms: ^{3}He and ^{21}Ne are produced primarily from spallation of Mg, Al, Si, and, for just ^{3}He, O. In Gale crater rocks, these elements are mainly hosted in primary silicate phases such as pyroxene and feldspar (e.g., Bristow et al., 2018; Rampe et al., 2017). The production of ^{36}Ar occurs via capture of cosmogenic thermal neutrons by ^{35}Cl, forming ^{36}Cl, which undergoes beta decay to ^{36}Ar on a short timescale (∼300 kyr) relative to the ages reported here. Spallogenic ^{36}Ar is also produced, but due to the high concentration of Cl in Martian soil, ^{36}Cl decay is responsible for the vast bulk of ^{36}Ar in these samples (Farley et al., 2014; Rao et al., 2002). The majority of Cl (and therefore ^{36}Ar) in the samples is likely present in chloride and perchlorate salts, although minor amounts of detrital chlorapatite may also be present (Rampe et al., 2017; Sutter et al., 2017).

In terrestrial and meteorite studies, additional cosmogenic nuclides are often measured including spallogenic ^{38}Ar, ^{20}Ne, and ^{22}Ne (e.g., Wieler, 2002). Isobaric interferences prevent measure-

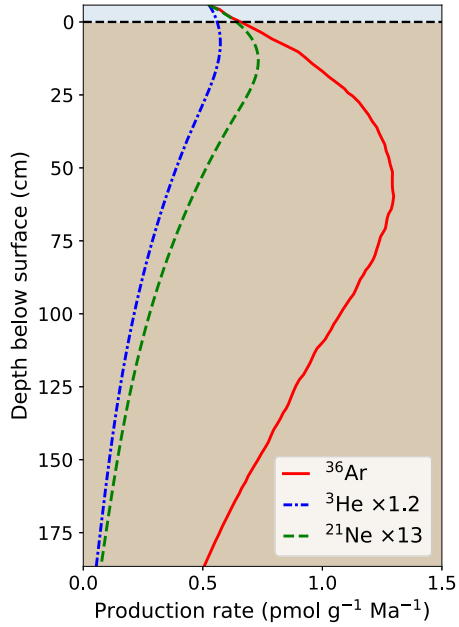

Fig. 2. Production of cosmogenic nuclides in the upper 2 m of the Martian subsurface based on the chemistry measured at Quela. The dashed horizontal line represents the surface; above this the nuclear cascade begins in the Martian atmosphere. Calculated using the rates given by (Wieler, 2002), the neutron flux from (Rao et al., 2002), and an assumed density of 2.6 g cm^{-3}. See Farley et al. (2014) for details of Martian cosmogenic nuclide production rate derivations.

ment of these additional isotopes: $H_2^{18}O$ dominates the m/z 20 signal, CO_2^{2+} overwhelms m/z 22, and the ^{38}Ar signal (which has no component resulting from neutron capture) is <<1% that of the isobaric $H^{37}Cl$ (Farley et al., 2014).

Interpretation of cosmogenic nuclide concentrations in the deep past relies on the assumption of an invariant flux of GCRs through time. Analysis of radioactive cosmogenic nuclides with varying half-lives suggests that on timescales up to a billion years the GCR flux is stable to within a factor of two (Wieler et al., 2013). We make the usual assumption that GCR flux is invariant through time, while recognizing that this has not been established with certainty.

Surface cosmogenic isotope concentrations can be interpreted via two endmember exposure scenarios: instantaneous exposure followed by negligible erosion, or steady state denudation (Lal, 1991). In the first model, exposure to cosmic rays begins when previously unexposed rock is rapidly exposed at the surface. Any geologically sudden unroofing event (e.g., scarp retreat, flood events, faulting, deglaciation) could cause such rapid exposure. In the case of instantaneous exposure, the sample has been exposed only at the surface (i.e., at a depth of 0 in Fig. 2). In the absence of any post-exposure cover, the cosmogenic isotope concentration at the surface (C_o) is therefore the product of the surface production rate (P_o) and the surface exposure age (τ), where the surface exposure age is the length of time elapsed since exposure at the surface began.

$$C_o = P_o \times \tau \quad (1)$$

In the second model, vertical denudation removes rock at a steady rate and the cosmogenic nuclide concentration in a sample at the surface represents the integration of nuclide production throughout the passage of the sample from depth to the surface. After steady-state is reached, this ultimately leads to a constant concentration profile. The subsurface production profile is not a smooth exponential curve, owing to the buildup of secondary particles in the shallow subsurface after primary cosmic ray bombardment of the thin Martian atmosphere (the nuclear cascade; Fig. 2). This production profile precludes the use of standard equations used to determine denudation rate in terrestrial studies (where the nuclear cascade occurs entirely in the atmosphere; e.g., Lal, 1991; Niedermann, 2002). We therefore constructed a numerical model to calculate a steady-state denudation rate using this more unusual profile. A description of the model is given in the supplementary information (S1.4); this model is used to calculate the maximum steady state denudation rates presented in Table 1.

Because spallogenic and neutron-capture isotopes have different production profiles with depth, their concentration ratio offers a clue as to which of the above endmember models, if either, has been active (Farley et al., 2014). Specifically, when the concentration of each cosmogenic nuclide is converted to an exposure age, if the ages of the spallogenic isotopes (^{3}He, ^{21}Ne) and the neutron capture isotope (^{36}Ar) are concordant, an instantaneous exposure scenario is supported. If the ^{36}Ar surface exposure age exceeds that calculated for the ^{3}He and ^{21}Ne, the relative cosmogenic nuclide abundances may be consistent with steady state denudation, or (depending on the exact concentration of each nuclide) may document a more complex erosion scenario.

The Cumberland and Windjana samples yielded internally consistent exposure ages for all three isotopes (Farley et al., 2014; Vasconcelos et al., 2016). The good agreement between the surface exposure ages for each of these rocks was taken as evidence that the local topography at both of these sites evolved recently via a geologically sudden exposure mechanism, most likely the retreat of small (a few meter-high) local scarps. This model is consistent with local geomorphology: Cumberland was drilled from a wide, flat basin surrounded by scarps, at the base of which erosional undercutting was prominent. At Windjana the drill location was on an exposed bench adjacent to the 3 m high Mt. Remarkable, a small butte close to two other similarly sized buttes.

Both vertical denudation and lateral scarp retreat have the net result of erosion, defined broadly as the net removal of rock. We use the term “denudation” to refer specifically to vertical surface lowering (via any mechanism, most commonly assumed to be eolian) and use the term “erosion” as an all-encompassing term to describe the net removal of rock which includes both vertical denudation and lateral scarp retreat.

2. Materials and methods

2.1. Sample descriptions

The Mojave 2 sample was collected from the lowermost exposed portion of the Murray formation at a site named Pahrump Hills. As the bedding in Gale crater does not display dips of greater than a few degrees (Stein et al., 2020), elevation can be used as a proxy for stratigraphic height: Mojave 2 is approximately 60 m in elevation above the Cumberland sample and 20 m above the Windjana sample. The chemistry and mineralogy of Mojave 2 were described previously (Table S2; Martin et al., 2017; Rampe et al., 2017). K-Ar results from Mojave 2 revealed that it contains young (2.12±0.36 Ga) jarosite and much older (4.07±0.63 Ga) plagioclase (Martin et al., 2017), consistent with an extended history of fluid flow and a detrital component concordant with the ancient formation age of detrital sediment measured at Cumberland (Farley et al., 2014). Mojave 2 is situated in a topographic low, 40 m from the nearest scarp, which is ~4.5 m high, has gently sloping sides, and is capped by the Stimson formation (Fig. 3). Based on planar projection from limited visual exposures ~40-90 meters distant, Mojave 2 is inferred to lie about five meters below the Murray-Stimson contact. However, this contact undulates by as much as 10 vertical meters over distances <200 m (Watkins et al., 2016). Mojave 2 could therefore be located just below the Siccar Point

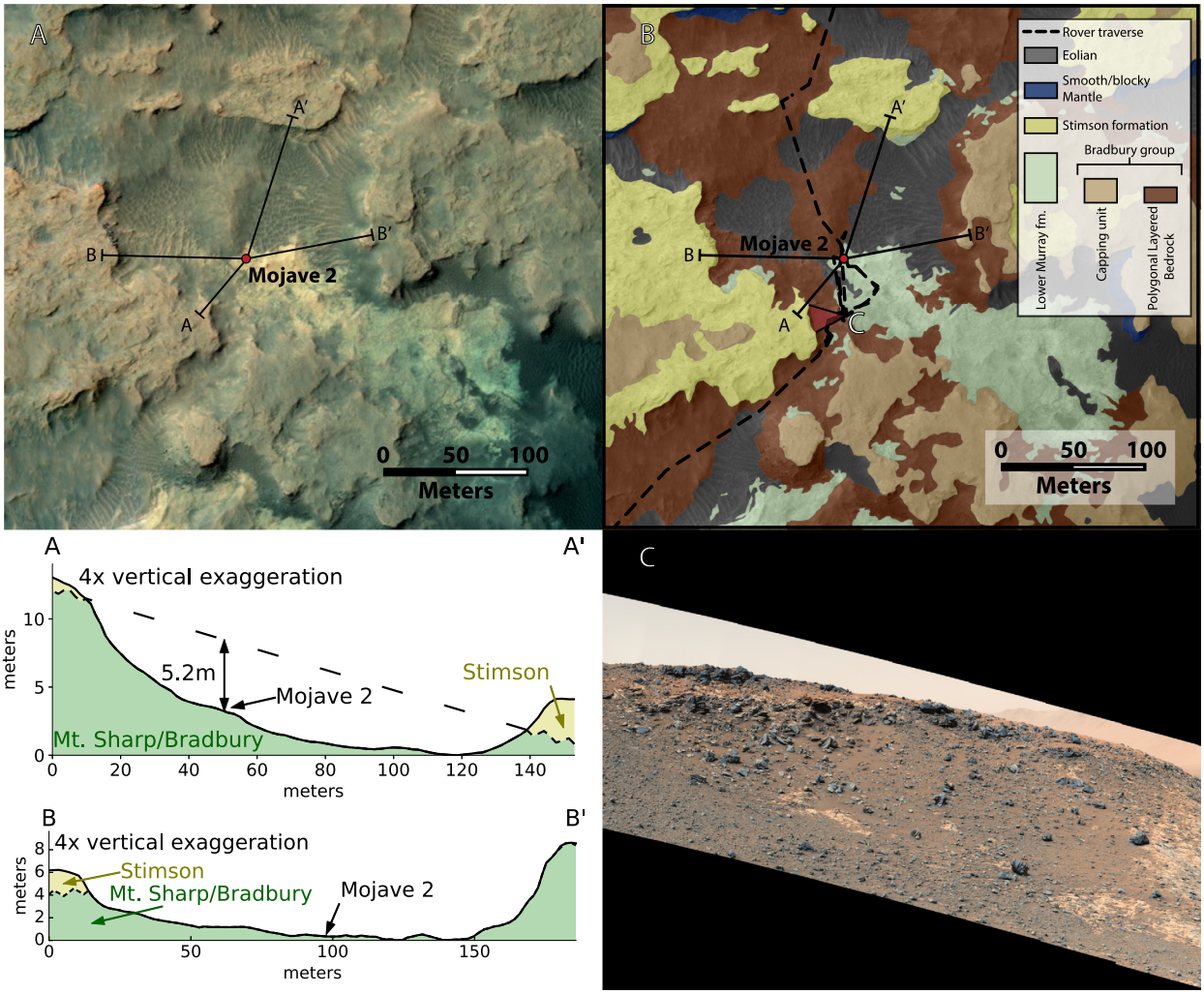

Fig. 3. A) Color image of the Mojave 2 sample site, with cross sections showing the topographic profile of the area and the location of the nearest Murray-Stimson contacts. North is up. B) Geologic map of the Pahrump hills; part (C) image location shown with red triangle. C) Mastcam mosaic (sol 907 100 mm 03970) of the Murray-Stimson contact at the southwest portion of the Pahrump Hills. (For interpretation of the colors in the figure(s), the reader is referred to the web version of this article.)

unconformity, or it could have been buried up to ~15 m below it when Stimson formation deposition began.

The Quela sample was also collected from the Murray formation, in an area known as the Murray buttes, ~80 m stratigraphically above Mojave 2 (100 m above Windjana and 140 m above Cumberland). Quela's mineralogy and chemistry are shown in Table S3. Given that this sample contains 2.3 wt% sanidine (Bristow et al., 2018), and previous work demonstrated that sanidine-bearing samples are not amenable to ^{40}Ar extraction using SAM (Vasconcelos et al., 2016), we do not report the K-Ar results for this sample. Much like the Pahrump Hills locality, the Murray buttes are erosional remnants (7-17 meters tall) capped by Stimson formation rocks. Quela was collected approximately five meters from the base of a butte (Fig. 4), and 1.3 m below the base of this talus-covered layer. Due to a covered interval of talus at the base of each butte, the Stimson makes up an unknown proportion of the stratigraphy of each butte. Close examination of the north side of the butte nearest Quela reveals that cross-bedded Stimson formation rocks protrude through the talus (Fig. 4c). We interpret this observation as evidence that the entirety of the covered interval is composed of Stimson at this site. Mapping the edge of the covered interval as the Murray-Stimson contact reveals an unconformity surface that dips slightly northward. Taking an upper limit of a planar projection of this surface and a lower limit of a horizontal projection of the edge of the talus covered slope, Quela lies 1.3-1.8 m below the Siccar Point unconformity.

2.2. Methods

The SAM analysis procedures used for the Quela measurement followed those developed by Farley et al. (2014). For Mojave 2, updated procedures described by Martin et al. (2017) were used. Briefly, 135±18 mg aliquots of samples collected from 2-5 cm depth were heated to ~930°C, releasing volatiles held within the samples. A semi-static measurement mode was employed to allow buildup of noble gases while reactive species were drawn down on a scrubber and getter within the gas handling line. The masses of interest (m/z 3, ^{3}He; m/z 21, ^{21}Ne; m/z 36, ^{36}Ar) were corrected for isobaric interferences and for background measured after the mass spectrometer was evacuated. Isobar correction was accomplished by regression against tracing gases at a known ratio to the gas of interest (e.g., $H^{37}Cl$ is used to correct for $H^{35}Cl$ to determine the ^{36}Ar signal). These isobaric gases comprise approximately 20% of the m/z 3 signal, 30% of m/z 21, and 95% of m/z 36. Although the corrections for isobaric interference are quite large, the uncertainty in the corrections is captured in the precision of the regressions and fully propagated into the estimated amount of each cosmogenic nuclide. Raw counts were averaged over the stable portion of the semi-static measurement and converted to

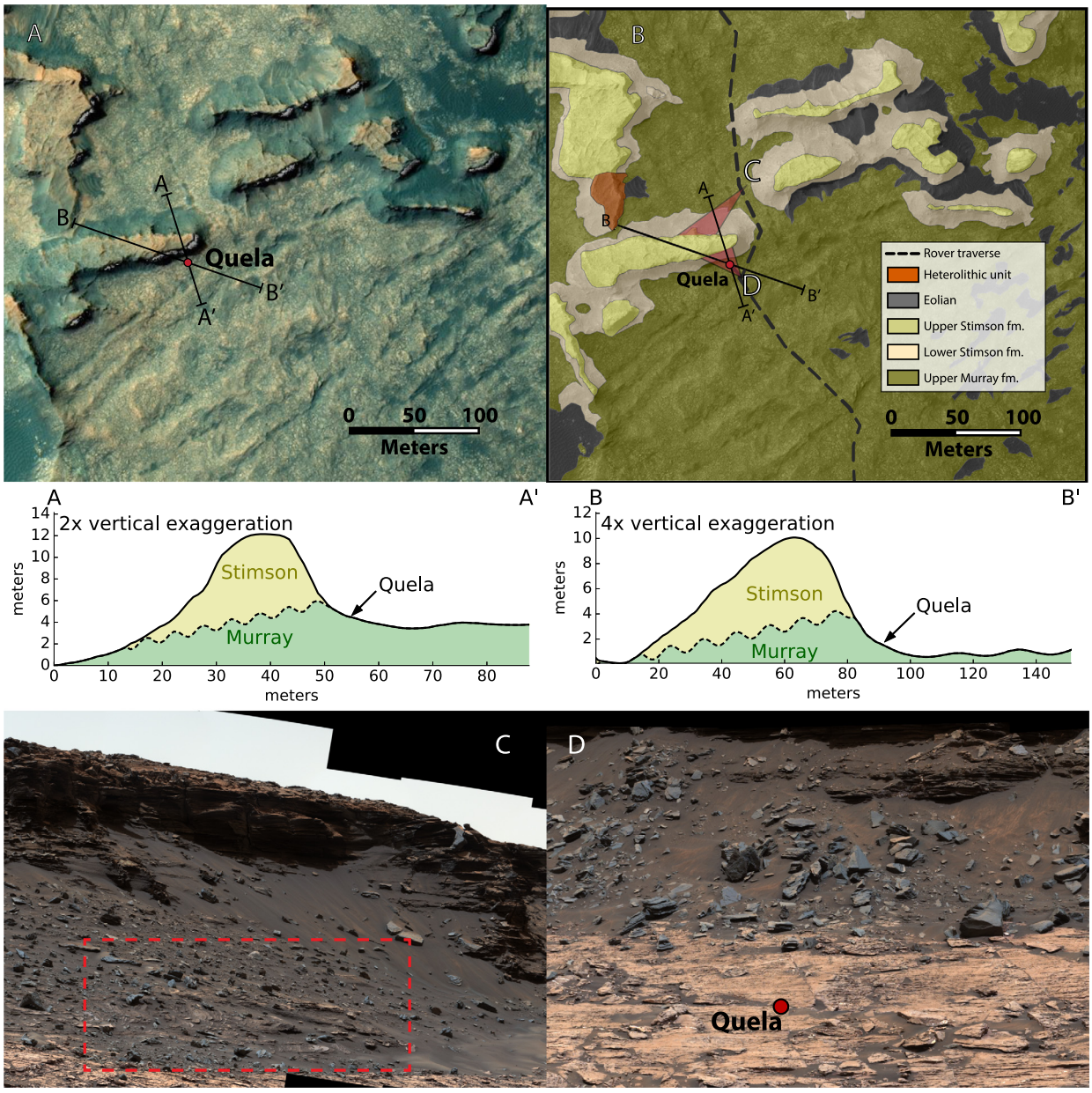

Fig. 4. A) Color image of the Quela sample site. Cross sections show the approximate location of the Murray-Stimson contact. North is up. B) Geologic map of the southern Murray buttes; Mastcam mosaic locations are shown with red triangles. C) Mastcam mosaic (sol 1450 100 mm 07179) acquired from the north side of the butte where Quela was collected (imaging location shown in panel B). Cross-strata are shown in the red highlight box indicating that the Murray-Stimson contact extends to the bottom of the Murray Buttes. D) Quela's drill location in Mastcam mosaic (sol 1455 34 mm 07197) on the south side of the butte shown in (C).

molar amounts using a known basic sensitivity, accounting for the enhancement in signal in "semi-static" mode relative to "dynamic" mode (Farley et al., 2014). This sensitivity was calibrated before launch and has been monitored for change by periodic atmospheric measurements of ^{40}Ar, which has a largely invariant partial pressure in the Martian atmosphere. No calibration gas standard is carried onboard the instrument. Cosmogenic isotope production rate calculations for each isotope are dependent on the chemical composition of the samples (Tables S2 & S3; Farley et al., 2014). A detailed description of the noble gas quantification for each sample is given in the Supplementary Material.

The uncertainty associated with each cosmogenic isotope concentration incorporates uncertainties associated with signal and isobar peak heights, regressions for isobar correction, background subtraction, and mass delivery. Uncertainties in surface production rates result only from uncertainties in bulk chemistry measurements; these are negligible and are therefore not included. Uncertainties were computed using a Monte Carlo model. All uncertainties reported here are at the 1σ level.

3. Results

Table 1 gives the cosmogenic nuclide concentrations for each sample and converts them to both surface exposure age and steady-state mean denudation rate assuming each isotope is purely cosmogenic in origin (see Section 4.1). The Mojave 2 ^{3}He and ^{21}Ne exposure ages (1,320±240 and 910±420 Ma respectively) agree within uncertainty, giving an error-weighted mean exposure age of 1,060±330 Ma. The ^{36}Ar released from Mojave 2 gives a surface exposure age of about 310±60 Ma, significantly younger than either ^{21}Ne or ^{3}He. The ^{3}He exposure age measured on Quela of 1,460±200 Ma is concordant with the ^{3}He and ^{21}Ne exposure ages

Table 1
Results of the noble gas experiment on Mojave 2 and Quela, with production rates and calculated ages. ^{21}Ne and ^{36}Ar could not be determined for Quela (see text).

	Mojave 2			Quela
	^{3}He	^{21}Ne	^{36}Ar	^{3}He
Gas amount (pmol g^{-1})	615±110	47±22	90±17	668±93
Surface production rate (pmol g^{-1} Ma^{-1})	0.4653	0.0523	0.2892	0.4566
Maximum Exposure Age (Ma)	1,320±240	910±420	310±60	1,460±200
Maximum Mean Denudation Rate (μm Ma^{-1})	710±130	1250±590	-	650±90

on Mojave 2. The ^{21}Ne and ^{36}Ar measurements from Quela have large isobaric interferences that preclude their use in this study (see S1.3 for details).

4. Discussion

Mojave 2 and Quela have far higher concentrations of cosmogenic nuclides than observed in the Cumberland and Windjana samples (Farley et al., 2014; Vasconcelos et al., 2016) and, unlike these previous studies, have discordant ^{3}He and ^{21}Ne compared to ^{36}Ar. These discrepancies raise the possibility that non-cosmogenic noble gases have been included in the samples. Here we explore alternative potential sources of these noble gases, and discuss the likely causes of the discordancy in ^{36}Ar.

4.1. Potential non-cosmogenic sources of ^{3}He and ^{21}Ne

Interplanetary dust particles (IDPs) have extremely high concentrations of implanted solar wind ^{3}He (Pepin et al., 2000) and could potentially contribute to the high ^{3}He concentrations measured in Mojave 2 and Quela. However, the ^{3}He/^{21}Ne ratio of 13±6 in Mojave 2 is consistent with the predicted spallogenic production ratio of 9, and is orders of magnitude lower than the ^{3}He/^{21}Ne ratio of ∼10^{5} found in IDPs (Pepin et al., 2000), inconsistent with an IDP origin for the vast bulk of the ^{3}He in the sample. Although the ^{21}Ne for Quela is unavailable for comparison, by analogy to Mojave 2, Cumberland, and Windjana, we argue that Quela is also unlikely to host significant quantities of IDPs as its lithology, mineralogy, and chemistry are not significantly different from these other samples (Table S3; Bristow et al., 2018; Farley et al., 2014; Martin et al., 2017; Rampe et al., 2017).

Another potential source of noncosmogenic He and Ne in these samples is meteoritic material carrying cosmogenic noble gases (Wieler, 2002). Iron meteorites have been observed directly on Mars (Schröder et al., 2008). Iron meteorites, devoid of a productive target for ^{21}Ne production, would carry a ^{3}He/^{21}Ne ratio of approximately 85, inconsistent with the observed ratio of 13±6 in Mojave 2. Furthermore, because neither Mojave 2 nor Quela has anomalously high Fe, the inclusion of iron meteorite material in either is unlikely. Cosmogenic noble gases in silicate meteorite material would likely be isotopically indistinguishable from such gases formed *in situ* on Mars, meaning that the inclusion of such material would not be obvious from noble gas data. Because impacts and collisions rapidly erode stony meteorites in space, their surface exposure ages are almost always <100 Ma (Wieler, 2002). Thus, even inclusion of an unreasonably high proportion (tens of percent) of meteoritic material cannot explain the high ^{3}He concentrations in Quela or Mojave 2.

Like previous workers (Farley et al., 2014; Vasconcelos et al., 2016), we assume that atmospheric noble gases are negligible in these analyses. Coupled with the above considerations, we conclude that the observed ^{3}He and ^{21}Ne are cosmogenic in origin, and that they reflect the integrated exposure history of the analyzed rock and/or its constituent detrital mineral grains.

4.2. Resetting of ^{36}Ar

Because it is formed from Cl and therefore in these sedimentary samples is held mostly in soluble phases like halite and perchlorate salts (Sutter et al., 2017), cosmogenic ^{36}Ar can potentially be released during interaction with even minor amounts of liquid water. This would decouple cosmogenic ^{36}Ar from the cosmogenic ^{3}He and ^{21}Ne dominantly carried in silicate grains. There is no erosion scenario that permits the low ratio of ^{36}Ar to ^{3}He and ^{21}Ne observed in Mojave 2, suggesting that it reflects either total aqueous resetting or, more likely, partial resetting at some unknown time or times in the past. Previous work has suggested transient liquid water at and near the surface of Mars during the Amazonian period (Cull et al., 2010), including in Gale crater (Anderson and Bell, 2010; Grant et al., 2014; Grant and Wilson, 2019; Martin et al., 2020; Palucis et al., 2016, 2014), and in the Mojave 2 sample itself (Martin et al., 2017). The observation of ^{36}Ar resetting is consistent with these previous studies. Recent work also shows that the perchlorate in Gale crater rocks is most likely post-depositional and was added during the Amazonian (Martin et al., 2020). If this perchlorate was added during the last 300 Ma, the young ^{36}Ar age could, in part, be due to the young formation age of some of the Cl-bearing salts containing ^{36}Ar. We therefore interpret ^{36}Ar independently from ^{3}He and ^{21}Ne.

The likely resetting of ^{36}Ar precludes the direct inference of erosional style responsible for exposure of the samples newly presented here. Unlike the case for Cumberland and Windjana (Farley et al., 2014; Vasconcelos et al., 2016), there is thus no reason to favor a scarp retreat model over a vertical denudation model on the basis of cosmogenic noble gas concentrations. The denudation rates calculated in Table 1 are sufficiently low that steady state would take ∼5.6 Ga to reach and therefore cannot have yet been achieved. We accordingly utilize the numerical model mentioned in Section 1.2 for such a transient case. Rather than assuming a steady-state condition, by asserting a most recent major erosion event at 3 Ga (i.e., resetting the cosmogenic nuclide concentrations to zero throughout the subsurface profile), an average denudation rate of ∼940 μm Ma^{-1} is derived based on the observed ^{3}He and ^{21}Ne concentrations. This rate is not significantly different from the average of 980±300 μm Ma^{-1} calculated assuming a steady-state profile (Table 1). As a shorthand for the length of time these samples have been exposed to cosmic rays, we discuss the cosmogenic nuclide concentrations in terms of exposure age below, acknowledging that this may not fully capture the erosion history of the samples.

5. Erosion and exposure history of Mount Sharp

In this section, we discuss geological scenarios that could result in the observed concentrations of cosmogenic ^{3}He and ^{21}Ne. As the total cosmogenic nuclide concentration in each grain represents the integrated exposure history of that grain, the interpretations presented here are endmember cases. We discuss each scenario by considering the likelihood that the bulk of the cosmogenic nuclide burden was imparted in that scenario, recognizing that the true history is potentially some combination of these endmembers.

5.1. Pre-depositional exposure

One potential explanation for the high concentration of cosmogenic noble gases in the two samples from Mount Sharp (Mojave 2 and Quela) relative to the two from Aeolis Palus (Cumberland and Windjana) is pre-depositional exposure. In this scenario, the

detrital components in Mojave 2 and Quela were exposed to cosmic ray irradiation for an extended period of time in an outcrop at the sediment source, as loose sediment during transport, and/or during any temporary storage before final deposition. After deposition in a lake within Gale crater, sediment grains would have been rapidly shielded from continuing buildup of cosmogenic noble gases initially by the water column, and soon afterwards by layers of sediment.

Such long exposure for grains that were eventually deposited in a basin implies that they must have been entirely eroded from the near surface (to allow for high rates of nuclide production) and either exposed in primary outcrop for ∼1 Ga, or their transport as sediment lasted a similar amount of time. This length of exposure requires that the sediments were exposed for the first billion years of Martian history, during a period of higher impact cratering rates and ejecta emplacement, as well as an overall more active geological setting (volcanism, fluvial and eolian processes, etc.). Such a history is implausible, especially compared with the possibility of extended exposure during the less active Amazonian period. Purely pre-depositional exposure is therefore an unlikely explanation for the high abundance of cosmogenic noble gases.

5.2. Murray-Stimson paleosurface exposure

The presence of the erosional unconformity between the Murray and Stimson formations indicates that deposition of the Stimson formation postdates the deposition, lithification, and paleoexposure of the Murray formation (Fig. 1; Banham et al., 2018; Fraeman et al., 2016). The length of time between Murray formation erosion and Stimson formation deposition is unknown (Banham et al., 2018). As both Mojave 2 and Quela are close to this contact, these samples could illuminate the length of time represented by the Siccar Point unconformity if they were exposed at or very near the paleosurface before Stimson deposition and later re-exposure. In this paleosurface exposure scenario, both Quela and Mojave 2 would have been exposed for ∼1 Ga between the time of Murray erosion and Stimson deposition, which would indicate that there was a long hiatus following the erosion of Mount Sharp group rocks to the level of the Siccar Point unconformity and the subsequent deposition of the Siccar Point group and the Stimson formation within it.

As the e-folding depth of cosmogenic nuclide production is 70 cm and the nuclear cascade is generated in the top ∼30 cm of rock, such a possibility requires that the rocks sampled at both Mojave 2 and Quela were located within ∼1 m of this paleosurface, where cosmogenic nuclide production would not be significantly inhibited (Fig. 2; Farley et al., 2014; Wieler, 2002). For Quela, such shallow depth is precluded. As discussed in Section 2.1, Quela was probably 1.3-1.8 meters below the contact (Fig. 4). Based on nearby exposures of the Siccar Point unconformity, Mojave 2 was also likely >1 m beneath the paleosurface (Fig. 3).

There is no independent reason to expect a long interval of surface exposure prior to Stimson deposition. No regolith, paleosol, ferrizone, or silcrete occurs at the Murray-Stimson contact (e.g., Newsom et al., 2018). Although it cannot be eliminated conclusively, a paleoexposure endmember is not the most parsimonious interpretation for these data.

5.3. Modern exposure

As paleosurface exposure appears unlikely, the most straightforward explanation for the exposure age results obtained for Mojave 2 and Quela is that both have been exposed to cosmic ray irradiation for the most recent ∼1 Ga. The geomorphology of the sample sites combined with this age may therefore yield insight to the mechanisms responsible for the generation of fresh surfaces at these locations. In the following sections, we first discuss the potential impact of post-erosional cover by unlithified sediment on the ages presented here, then the likely style of landscape change, and finally the implications for the long-term evolution of Mount Sharp.

5.3.1. Post-erosion cover

Wiens et al. (2020) describe localized patches of sediment tens to hundreds of meters in spatial extent, occurring along the lower northern slopes of Mt. Sharp. Rover inspection of three of these patches revealed they are poorly sorted (fine gravel to boulders) unconsolidated sediment occurring as thin deposits overlying the Murray eroded surface, and locally onlapping the Stimson. The sediment is derived from sandstone and conglomerates of varying composition. Mojave 2 and Quela are both located within ∼500 m of these deposits. Wiens et al. (2020) concluded that the deposits post-date the deposition and erosion of the Stimson formation. In Fig. 4, the beginning of cross-section B is on the northern tip of a deposit that appears similar to these heterolithic units in HiRISE and Mastcam images. This raises the possibility of a period of time when there may have been scour and deposition (and thus burial) on the Murray surface in this area, although these deposits do not presently define a continuous field of sediment cover on the Murray surface.

The consequence of burial would be to cease (or slow) isotopic production until erosion re-exposed the surface. This change in cosmogenic nuclide production would result in exposure ages which underestimate the actual age of the surfaces where Quela and Mojave 2 were collected. A similar age gap would arise if Bagnold dune sands ever covered these sites. Presently there is no direct evidence of burial at these sites, either by gravel or sand, though evidence for both occurs nearby. If the sample sites at Mojave 2 and Quela were buried by unlithified sediment, the overall effect would be that the ages discussed here would be underestimates and the final conclusions of this work would be unaffected or strengthened.

5.3.2. Landform generation

It has been proposed that impact cratering, fluvial, and wind processes initiated incision through Stimson rocks to the Murray formation (Wiens et al., 2020), followed by widening of valley floors via lateral migration of the resulting scarps. Typically, the Stimson forms cliffs below which blocks derived from the cliff have accumulated on the less-steep basal slope (e.g., Fig. 4c; Banham et al., 2018). Blocks derived from the Stimson extend down to the valley floor where their size and number quickly decline across the floor away from the escarpment. A few blocks are commonly found 10s of meters from the escarpment base (Fig. 3c and figures within Banham et al., 2018). There is no apparent mechanism to deliver blocks this far from the scarps, suggesting instead that they are remnant blocks left over from the scarp retreat process.

While erosional style cannot be directly ascertained from the noble gas data (i.e., instantaneous exposure vs. vertical denudation; Sections 1.2 and 4.2), the geomorphology of the Quela site could be interpreted to suggest that scarp retreat is responsible for exposure of that sample. A scarp eight meters tall exists approximately five meters from Quela (Fig. 4), a geometry that is unlikely to have arisen purely by vertical denudation. The sampling site of Mojave 2 lies in a bowl-shaped depression at the base of ∼17-degree hillslopes that rise up over 10 m to the south (Fig. 3). The hillslope form indicates lateral retreat towards the south, but denudation (vertical incision) may have played an additional minor role in the exposure of this sample at the surface.

At both localities, then, scarp retreat has apparently occurred, although the details regarding how scarp retreat took place remains unknown, and whether scarp retreat continues to this day

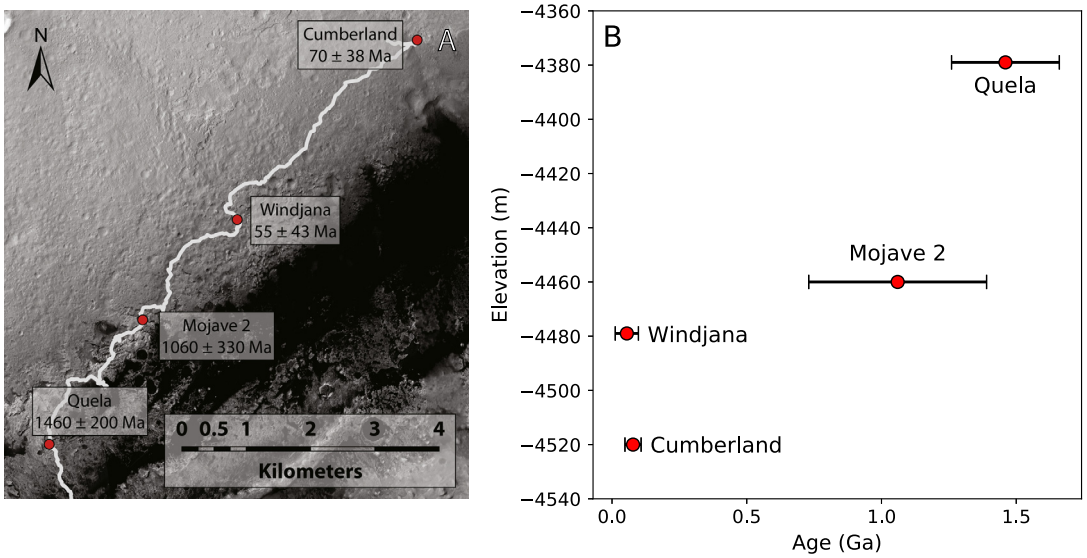

Fig. 5. A) Map of sample locations with error-weighted mean exposure age of each sample shown. B) Error-weighted mean ages of each exposure age so far measured by SAM plotted against elevation below the Mars geoid.

or these landforms are relict from earlier events cannot be directly assessed from the geochemical data. Fluvial incision can cut steep canyon walls, but is unlikely to then sweep laterally great distances (leading to mesas separated by tens to hundreds of meters, as found at Quela) and leave a relatively smooth floor with no trace of channel processes. Such incision would also have been recorded downslope in large deposits of sediment, which are not observed. After incision through the Stimson to the Murray, the landscapes observed at Mojave 2 and Quela may therefore have arisen purely from mass movement and eolian processes, as the scarps initially produced via vertical incision migrated laterally.

Of the samples measured, two pairs of concordant exposure ages are observed: Cumberland and Windjana, which have been exposed for <100 Ma, and Mojave 2 and Quela, which have been exposed for ∼1 Ga (Fig. 5b). There are three scenarios that plausibly account for these observations: 1) vertical denudation, 2) steady scarp retreat, or 3) episodic, rapid scarp retreat. Based on the above description of geomorphology, the first option is unlikely.

The diverse topography of the Gale crater floor and the slopes of Mt. Sharp indicate that erosion has varied greatly across this landscape. The two younger exposure ages and two older exposure ages may simply record differing ongoing local erosion rates (option 2 above). Such differences could be driven by differences in winds, sediment supply (for abrasion), and rock hardness. An additional factor may be the local height of the retreating feature that led to surface exposure. In both the young ages, lateral retreat has been hypothesized to be associated with relatively small (less than a few meters) topographic steps (Farley et al., 2014; Vasconcelos et al., 2016). In contrast, the total mass erosion needed to cause retreat would be much greater to displace the ∼10 m high boulder-mantled slopes facing Quela and Mojave 2. In this case, variability of age/scarp retreat rate potentially arises from the topographic scale of the retreating feature. Such a model suggests that local rock properties and a sample's location within Gale crater are the determining factors in its exposure age and, by proxy, the scarp retreat/erosion rate of that locality.

Another possibility is that the clustering of ages observed by the Curiosity rover (Fig. 5; Farley et al., 2014; Vasconcelos et al., 2016) indicate discrete episodes of increased erosion relative to typical Amazonian erosion rates, leading to relatively brief intervals of intense scarp retreat and common exposure ages. Such a scenario would imply that erosion events localized by geomorphology and/or rock properties cause the shared exposure ages, though exactly how the surfaces at Mojave 2 and Quela survived the putative later erosive event at Cumberland and Windjana is unclear. These events could occur during periods of unusual obliquity and/or during uniquely strong windstorm events, recurring on timescales of hundreds of millions of years. This interpretation fits into a larger theme observed across Mars and throughout the preserved geologic record of multiple, discrete fluvial erosion episodes contributing to observed geomorphology (e.g., Kite, 2019). While we propose that the landforms under study here arose via mass movement and eolian processes, a similar model could be applicable in which specific criteria (e.g., orbital mechanics, volcanism, dust storm activity) align to permit conditions that allow brief but intense erosional periods to arise.

5.3.3. *Formation of Mount Sharp and history of Gale crater*

The longer exposure ages on Mount Sharp (Mojave 2 and Quela) relative to those on Aeolis Palus (Cumberland and Windjana) might indicate a differential rate of rock removal which could partially explain the creation of the depression between Mount Sharp and the crater rim. However, based on the long exposure ages calculated here, the effective modern erosion rate is insufficient to explain the erosional evolution of Mount Sharp to its present form. The scarp migration rate implied by the presence of a large scarp 5 meters from Quela, which has been exposed for over 1 Ga, indicates that ongoing erosion is negligible and cannot even explain the hundreds of meters separating buttes in the area. Given that modern erosion rates are clearly insufficient to have formed Mount Sharp, erosion must have been more rapid in the past. Slowing erosion as a function of time could be a result of atmospheric loss (Armstrong and Leovy, 2005; Grotzinger et al., 2015; Jakosky et al., 1994), if only the rate, and not the style or location, of erosion has changed. In addition, as sediment has preferentially been removed from Gale crater (indicated by the erosion of the Stimson formation and scouring of the crater floor), the loss of sand as abrading agent may also play a role in slowing erosion.

Another consideration is that an exposure age provides a lower limit on the length of time a given sample has been exposed to cosmic rays (Section 1.2). If any component of vertical denudation is present in the erosion mechanism, the surfaces at Mojave 2 and Quela would have been exposed for even longer than calculated in Table 1. Asserting an erosion event timing of 3 Ga, a denudation rate of ∼0.94 m Ga^{-1} is derived for both Mojave 2 and Quela (as

discussed in Section 4.2), far too slow to explain the formation of Mount Sharp if this rate were not significantly greater in the past.

Estimated rates of surface lowering rates on Mars vary between 100 m Ga^{-1} (Kite and Mayer, 2017) and 0.01 m Ga^{-1} (Golombek and Bridges, 2000). Regardless of the processes that formed Mount Sharp, these modern erosion rates imply that, for the observed landforms in Gale crater (including Mount Sharp) to have emerged, the rate of landscape change must have been far greater in the distant past than in the more recent past. This conclusion suggests that Mount Sharp had largely or entirely formed before the start of the Amazonian, consistent with crater count and morphology studies (Grant et al., 2014; Le Deit et al., 2013; Palucis et al., 2014; Thomson et al., 2011). Given the implied extremely slow rates of landscape change, the scarp retreat observed at the sample sites discussed here is most likely only a minor, second-order effect on the first-order topography of Mount Sharp and the mantling units that cover it. Mount Sharp therefore has likely existed in nearly its current form since the Hesperian.

6. Conclusions

The first samples from Mount Sharp strata analyzed for cosmogenic noble gas content yielded exposure ages far older than those from the surrounding plains of Aeolis Palus. Mojave 2 gave a ^{3}He age of 1,320±240 Ma, ^{21}Ne of 910±420 Ma, and ^{36}Ar of 310±60 Ma. A cosmogenic ^{3}He age of 1,460±200 Ma was observed in the sample Quela; ^{21}Ne and ^{36}Ar could not be quantified due to uncorrectable isobaric interference. The relative youth of the calculated ^{36}Ar age in Mojave 2 may result from resetting (or partial resetting) during a transient wetting event, consistent with previous studies. The spallation nuclides ^{3}He and ^{21}Ne are held mostly in insoluble silicate grains and likely reflect the total accumulated exposure history of the two samples.

Neither pre-depositional exposure nor paleoexposure at the Siccar Point unconformity are plausible scenarios to explain the high concentration of cosmogenic noble gases in these samples. Instead, the most straightforward interpretation of the data is that the mudstones sampled at Mojave 2 and Quela have been exposed for the most recent ∼1 Ga. The lack of geologically meaningful ^{36}Ar data precludes the direct determination of scarp retreat vs. vertical denudation as endmember models of erosion mechanism. However, the geomorphic setting of Quela practically requires butte-forming scarp retreat to have been the major mode of landscape change. Mojave 2 is more likely to have had minor contributions of denudation, but also seems likely to have been largely exposed by scarp retreat. Taken together with the data from Cumberland and Windjana, we suggest that scarp retreat remains an overall slow but active process, with significant topographic change caused by brief periods of rapid erosion (relative to typical modern rates) in discrete areas of Gale crater.

The contrast between the ∼1 Ga exposure age of Quela and Mojave 2 and the <100 Ma exposure ages obtained from samples from Aeolis Palus might reflect differences in rock types and height of scarps, but also likely records differences associated with wind and sand supply patterns. Scarp retreat likely varies with changes in atmospheric conditions and thus wind erosion intensity. While the younger exposure ages on Aeolis Palus than Mount Sharp could indicate excavation of the crater floor, the length of exposure observed at these sites precludes an erosive origin of Mount Sharp via modern erosion rates and mechanisms. It is therefore likely that Mount Sharp had been eroded to nearly its current form before the Amazonian Period began, and has since undergone relatively minor erosion.

CRediT authorship contribution statement

Peter E. Martin: Conceptualization, Formal analysis, Investigation, Methodology, Software, Visualization, Writing – original draft, Writing – review & editing. **Kenneth A. Farley:** Conceptualization, Funding acquisition, Methodology, Project administration, Supervision, Writing – original draft, Writing – review & editing. **Charles A. Malespin:** Conceptualization, Data curation, Investigation, Methodology, Resources. **Paul R. Mahaffy:** Data curation, Funding acquisition, Investigation, Project administration, Resources. **Kenneth S. Edgett:** Writing – original draft. **Sanjeev Gupta:** Writing – original draft. **William E. Dietrich:** Writing – original draft. **Michael C. Malin:** Conceptualization, Writing – original draft. **Kathryn M. Stack:** Writing – original draft. **Paulo M. Vasconcelos:** Conceptualization, Methodology.

Declaration of competing interest

The authors declare that they have no known competing financial interests or personal relationships that could have appeared to influence the work reported in this paper.

Acknowledgements

We thank the SAM, CheMin, and APXS teams and other MSL team members for their operational support, without which these data could not have been generated. Thanks also to Jay Dickson for assistance with file handling, logistical, and figure-making support. The data contained in this manuscript are archived with the NASA Planetary Data System (PDS; SAM: https://pds-geosciences.wustl.edu/missions/msl/sam.htm; APXS: https://pds-geosciences.wustl.edu/missions/msl/apxs.htm). This work was supported by a NASA participating scientist grant to KAF. KMS participated in this project at the Jet Propulsion Laboratory, California Institute of Technology, under a contract with the National Aeronautics and Space Administration (80NM0018D0004). SG acknowledges funding from the UK Space Agency (UKSA) (Grant numbers: ST/N000579/1; ST/S001492/1).

Appendix A. Supplementary material

Supplementary material related to this article can be found online at https://doi.org/10.1016/j.epsl.2020.116667.

References

Anderson, R.B., Bell, J.F.I., 2010. Geologic mapping and characterization of Gale Crater and implications for its potential as a Mars Science Laboratory landing site. Mars 5, 76–128. https://doi.org/10.1555/mars.2010.0004.

Anderson, R.B., Edgar, L.A., Rubin, D.M., Lewis, K.W., Newman, C., 2018. Complex bedding geometry in the upper portion of Aeolis Mons, Gale crater, Mars. Icarus 314, 246–264. https://doi.org/10.1016/j.icarus.2018.06.009.

Armstrong, J.C., Leovy, C.B., 2005. Long term wind erosion on Mars. Icarus 176, 57–74. https://doi.org/10.1016/j.icarus.2005.01.005.

Arvidson, R., Guinness, E., Lee, S., 1979. Differential aeolian redistribution rates on Mars. Nature 278, 533–535. https://doi.org/10.1038/278533a0.

Banham, S.G., Gupta, S., Rubin, D.M., Watkins, J.A., Sumner, D.Y., Edgett, K.S., Grotzinger, J.P., Lewis, K.W., Edgar, L.A., Stack-Morgan, K.M., Barnes, R., Bell, J.F., Day, M.D., Ewing, R.C., Lapotre, M.G.A., Stein, N.T., Rivera-Hernandez, F., Vasavada, A.R., 2018. Ancient Martian aeolian processes and palaeomorphology reconstructed from the Stimson formation on the lower slope of Aeolis Mons, Gale crater, Mars. Sedimentology 65, 993–1042. https://doi.org/10.1111/sed.12469.

Bennett, K.A., Bell, J.F., 2016. A global survey of martian central mounds: central mounds as remnants of previously more extensive large-scale sedimentary deposits. Icarus 264, 331–341. https://doi.org/10.1016/j.icarus.2015.09.041.

Bristow, T.F., Rampe, E.B., Achilles, C.N., Blake, D.F., Chipera, S.J., Craig, P., Crisp, J.A., Marais, D.J.D., Downs, R.T., Gellert, R., Grotzinger, J.P., Gupta, S., Hazen, R.M., Horgan, B., Hogancamp, J.V., Mangold, N., Mahaffy, P.R., McAdam, A.C.,

Ming, D.W., Morookian, J.M., Morris, R.V., Morrison, S.M., Treiman, A.H., Vaniman, D.T., Vasavada, A.R., Yen, A.S., 2018. Clay mineral diversity and abundance in sedimentary rocks of Gale crater, Mars. Sci. Adv. 4, eaar3330. https://doi.org/10.1126/sciadv.aar3330.

Cull, S.C., Arvidson, R.E., Catalano, J.G., Ming, D.W., Morris, R.V., Mellon, M.T., Lemmon, M., 2010. Concentrated perchlorate at the Mars Phoenix landing site: evidence for thin film liquid water on Mars. Geophys. Res. Lett. 37. https://doi.org/10.1029/2010GL045269.

Day, M., Anderson, W., Kocurek, G., Mohrig, D., 2016. Carving intracrater layered deposits with wind on Mars. Geophys. Res. Lett. 43, 2473–2479. https://doi.org/10.1002/2016GL068011.

Day, M., Kocurek, G., 2016. Observations of an aeolian landscape: from surface to orbit in Gale Crater. Icarus, MicroMars to MegaMars 280, 37–71. https://doi.org/10.1016/j.icarus.2015.09.042.

Farley, K., Malespin, C., Mahaffy, P., Grotzinger, J., Vasconcelos, P., Milliken, R., Malin, M., Edgett, K., Pavlov, A., Hurowitz, J., 2014. In situ radiometric and exposure age dating of the Martian surface. Science 343, 1247166.

Fraeman, A.A., Ehlmann, B.L., Arvidson, R.E., Edwards, C.S., Grotzinger, J.P., Milliken, R.E., Quinn, D.P., Rice, M.S., 2016. The stratigraphy and evolution of lower Mount Sharp from spectral, morphological, and thermophysical orbital data sets. J. Geophys. Res., Planets 121, 1713–1736. https://doi.org/10.1002/2016JE005095.

Gellert, R., Clark, B.C., The MSL Team, 2015. In situ compositional measurements of rocks and soils with the Alpha Particle X-ray Spectrometer on NASA's Mars rovers. Elements 11, 39–44. https://doi.org/10.2113/gselements.11.1.39.

Golombek, M.P., Bridges, N.T., 2000. Erosion rates on Mars and implications for climate change: constraints from the Pathfinder landing site. J. Geophys. Res., Planets 105, 1841–1853. https://doi.org/10.1029/1999JE001043.

Grant, J.A., Wilson, S.A., 2019. Evidence for late alluvial activity in Gale Crater, Mars. Geophys. Res. Lett. 46, 7287–7294. https://doi.org/10.1029/2019GL083444.

Grant, J.A., Wilson, S.A., Mangold, N., Calef, F., Grotzinger, J.P., 2014. The timing of alluvial activity in Gale crater, Mars. Geophys. Res. Lett. 41, 1142–1149.

Grindrod, P.M., Warner, N.H., 2014. Erosion rate and previous extent of interior layered deposits on Mars revealed by obstructed landslides. Geology 42, 795–798. https://doi.org/10.1130/G35790.1.

Grotzinger, J., Gupta, S., Malin, M., Rubin, D., Schieber, J., Siebach, K., Sumner, D., Stack, K., Vasavada, A., Arvidson, R., 2015. Deposition, exhumation, and paleoclimate of an ancient lake deposit, Gale crater, Mars. Science 350, aac7575.

Jakosky, B.M., Pepin, R.O., Johnson, R.E., Fox, J.L., 1994. Mars atmospheric loss and isotopic fractionation by solar-wind-induced sputtering and photochemical escape. Icarus 111, 271–288. https://doi.org/10.1006/icar.1994.1145.

Kite, E.S., 2019. Geologic constraints on early Mars climate. Space Sci. Rev. 215, 10. https://doi.org/10.1007/s11214-018-0575-5.

Kite, E.S., Mayer, D.P., 2017. Mars sedimentary rock erosion rates constrained using crater counts, with applications to organic-matter preservation and to the global dust cycle. Icarus 286, 212–222. https://doi.org/10.1016/j.icarus.2016.10.010.

Kronyak, R.E., Kah, L.C., Edgett, K.S., VanBommel, S.J., Thompson, L.M., Wiens, R.C., Sun, V.Z., Nachon, M., 2019. Mineral-filled fractures as indicators of multigenerational fluid flow in the Pahrump Hills member of the Murray formation, Gale crater, Mars. Earth Space Sci. 6, 238–265. https://doi.org/10.1029/2018EA000482.

Lal, D., 1991. Cosmic ray labeling of erosion surfaces: in situ nuclide production rates and erosion models. Earth Planet. Sci. Lett. 104, 424–439. https://doi.org/10.1016/0012-821X(91)90220-C.

Le Deit, L., Hauber, E., Fueten, F., Pondrelli, M., Rossi, A.P., Jaumann, R., 2013. Sequence of infilling events in Gale Crater, Mars: results from morphology, stratigraphy, and mineralogy. J. Geophys. Res., Planets, 2439–2473. https://doi.org/10.1002/2012JE004322@10.1002/(ISSN)2169-9100.EARLYMARS3.

Mahaffy, P.R., Webster, C.R., Cabane, M., Conrad, P.G., Coll, P., Atreya, S.K., Arvey, R., Barciniak, M., Benna, M., Bleacher, L., 2012. The sample analysis at Mars investigation and instrument suite. Space Sci. Rev. 170, 401–478.

Malin, M.C., Edgett, K.S., 2000. Sedimentary rocks of early Mars. Science 290, 1927–1937. https://doi.org/10.1126/science.290.5498.1927.

Malin, M.C., Edgett, K.S., Posiolova, L.V., McColley, S.M., Dobrea, E.Z.N., 2006. Present-day impact cratering rate and contemporary Gully activity on Mars. Science 314, 1573–1577. https://doi.org/10.1126/science.1135156.

Martin, P.E., Farley, K.A., Archer, P.D., Hogancamp, J.V., Siebach, K.L., Grotzinger, J.P., McLennan, S.M., 2020. Reevaluation of perchlorate in Gale crater rocks suggests geologically recent perchlorate addition. J. Geophys. Res., Planets 125, e2019JE006156. https://doi.org/10.1029/2019JE006156.

Martin, P.E., Farley, K.A., Baker, M.B., Malespin, C.A., Schwenzer, S.P., Cohen, B.A., Mahaffy, P.R., McAdam, A.C., Ming, D.W., Vasconcelos, P.M., Navarro-González, R., 2017. A two-step K-Ar experiment on Mars: dating the diagenetic formation of Jarosite from Amazonian groundwaters. J. Geophys. Res., Planets 122, 2017JE005445. https://doi.org/10.1002/2017JE005445.

Milliken, R., Grotzinger, J., Thomson, B., 2010. Paleoclimate of Mars as captured by the stratigraphic record in Gale Crater. Geophys. Res. Lett. 37.

Newsom, H.E., Edgett, K.S., Fey, D.M., Frydenvang, J., Banham, S.G., Gupta, S., Williams, A.J., Grotzinger, J.P., Mangold, N., Schieber, J., Rivera-Hernandez, F., Belgacem, I., 2018. A buried aeolian lag deposit at an unconformity between the Murray and Stimson formations at Marias Pass, Gale Crater, Mars. In: Lunar and Planetary Science Conference, p. 2083.

Niedermann, S., 2002. Cosmic-ray-produced noble gases in terrestrial rocks: dating tools for surface processes. Rev. Mineral. Geochem. 47, 731–784. https://doi.org/10.2138/rmg.2002.47.16.

Palucis, M.C., Dietrich, W.E., Hayes, A.G., Williams, R.M.E., Gupta, S., Mangold, N., Newsom, H., Hardgrove, C., Calef, F., Sumner, D.Y., 2014. The origin and evolution of the Peace Vallis fan system that drains to the Curiosity landing area, Gale Crater, Mars. J. Geophys. Res., Planets 119, 705–728. https://doi.org/10.1002/2013JE004583.

Palucis, M.C., Dietrich, W.E., Williams, R.M.E., Hayes, A.G., Parker, T., Sumner, D.Y., Mangold, N., Lewis, K., Newsom, H., 2016. Sequence and relative timing of large lakes in Gale crater (Mars) after the formation of Mount Sharp. J. Geophys. Res., Planets 121, 472–496. https://doi.org/10.1002/2015JE004905.

Pavlov, A.A., Vasilyev, G., Ostryakov, V.M., Pavlov, A.K., Mahaffy, P., 2012. Degradation of the organic molecules in the shallow subsurface of Mars due to irradiation by cosmic rays. Geophys. Res. Lett. 39. https://doi.org/10.1029/2012GL052166.

Pepin, R.O., Palma, R.L., Schlutter, D.J., 2000. Noble gases in interplanetary dust particles, I: the excess helium-3 problem and estimates of the relative fluxes of solar wind and solar energetic particles in interplanetary space. Meteorit. Planet. Sci. 35, 495–504. https://doi.org/10.1111/j.1945-5100.2000.tb01431.x.

Rampe, E., Ming, D., Blake, D., Bristow, T., Chipera, S., Grotzinger, J., Morris, R., Morrison, S., Vaniman, D., Yen, A., 2017. Mineralogy of an ancient lacustrine mudstone succession from the Murray formation, Gale crater, Mars. Earth Planet. Sci. Lett. 471, 172–185.

Rao, M.N., Bogard, D.D., Nyquist, L.E., McKay, D.S., Masarik, J., 2002. Neutron capture isotopes in the Martian regolith and implications for Martian atmospheric noble gases. Icarus 156, 352–372. https://doi.org/10.1006/icar.2001.6809.

Schröder, C., Rodionov, D.S., McCoy, T.J., Jolliff, B.L., Gellert, R., Nittler, L.R., Farrand, W.H., Johnson, J.R., Ruff, S.W., Ashley, J.W., Mittlefehldt, D.W., Herkenhoff, K.E., Fleischer, I., Haldemann, A.F.C., Klingelhöfer, G., Ming, D.W., Morris, R.V., de Souza, P.A., Squyres, S.W., Weitz, C., Yen, A.S., Zipfel, J., Economou, T., 2008. Meteorites on Mars observed with the Mars exploration rovers. J. Geophys. Res., Planets 113. https://doi.org/10.1029/2007JE002990.

Stein, N.T., Quinn, D.P., Grotzinger, J.P., Fedo, C., Ehlmann, B.L., Stack, K.M., Edgar, L.A., Fraeman, A.A., Deen, R., 2020. Regional structural orientation of the Mt. Sharp group revealed by in-situ dip measurements and stratigraphic correlations on the Vera Rubin ridge. J. Geophys. Res., Planets 125, e2019JE006298. https://doi.org/10.1029/2019JE006298.

Sutter, B., McAdam, A.C., Mahaffy, P.R., Ming, D.W., Edgett, K.S., Rampe, E.B., Eigenbrode, J.L., Franz, H.B., Freissinet, C., Grotzinger, J.P., Steele, A., House, C.H., Archer, P.D., Malespin, C.A., Navarro-González, R., Stern, J.C., Bell, J.F., Calef, F.J., Gellert, R., Glavin, D.P., Thompson, L.M., Yen, A.S., 2017. Evolved gas analyses of sedimentary rocks and eolian sediment in Gale Crater, Mars: results of the Curiosity rover's sample analysis at Mars instrument from Yellowknife Bay to the Namib Dune. J. Geophys. Res., Planets 122, 2574–2609. https://doi.org/10.1002/2016JE005225.

Thomson, B.J., Bridges, N.T., Milliken, R., Baldridge, A., Hook, S.J., Crowley, J.K., Marion, G.M., de Souza Filho, C.R., Brown, A.J., Weitz, C.M., 2011. Constraints on the origin and evolution of the layered mound in Gale Crater, Mars using Mars Reconnaissance Orbiter data. Icarus 214, 413–432. https://doi.org/10.1016/j.icarus.2011.05.002.

Vasconcelos, P., Farley, K., Malespin, C., Mahaffy, P., Ming, D., McLennan, S., Hurowitz, J., Rice, M.S., 2016. Discordant K-Ar and young exposure dates for the Windjana sandstone, Kimberley, Gale Crater, Mars. J. Geophys. Res., Planets 121, 2176–2192.

Watkins, J.A., Grotzinger, J.P., Stein, N., Banham, S.G., Gupta, S., Rubin, D., Stack, K.M., Edgett, K.S., 2016. Paleotopography of erosional unconformity, base of Stimson Formation, Gale Crater, Mars. In: Lunar and Planetary Sciences Conference, p. 2939.

Wieler, R., 2002. Cosmic-ray-produced noble gases in meteorites. Rev. Mineral. Geochem. 47, 125–170. https://doi.org/10.2138/rmg.2002.47.5.

Wieler, R., Beer, J., Leya, I., 2013. The galactic cosmic ray intensity over the past 106–109 years as recorded by cosmogenic nuclides in meteorites and terrestrial samples. Space Sci. Rev. 176, 351–363. https://doi.org/10.1007/s11214-011-9769-9.

Wiens, R.C., Edgett, K.S., Stack, K.M., Dietrich, W.E., Bryk, A.B., Mangold, N., Bedford, C., Gasda, P., Fairen, A., Thompson, L., Johnson, J., Gasnault, O., Clegg, S., Cousin, A., Forni, O., Frydenvang, J., Lanza, N., Maurice, S., Newsom, H., Ollila, A., Payré, V., Rivera-Hernandez, F., Vasavada, A., 2020. Origin and composition of three heterolithic boulder- and cobble-bearing deposits overlying the Murray and Stimson formations, Gale Crater, Mars. Icarus 350, 113897. https://doi.org/10.1016/j.icarus.2020.113897.